PERGAMON

International Journal of Heat and Mass Transfer 44 (2001) 1171–1184

International Journal of HEAT and MASS TRANSFER

www.elsevier.com/locate/ijhmt

Isothermal and heated turbulent upflow in a vertical annular channel – Part I. Experimental measurements

S. Kang, B. Patil, J.A. Zarate, R.P. Roy *

Department of Mechanical and Aerospace Engineering, Arizona State University, Mail Station 6106, Tempe, AZ 85287-6106, USA

Received 28 September 1999; received in revised form 28 April 2000

Abstract

The velocity and thermal fields were measured in isothermal and heated turbulent upflow of liquid Refrigerant-113 through a vertical annular channel of inner to outer radius ratio 0.415. A two-component laser Doppler velocimeter was used for the velocity measurements and, simultaneously, a cold-wire for the temperature measurements. The dimensions of the LDV measuring volume and the cold-wire, and their proximity to each other were important considerations. Also crucial to the measurements were the LDV coincidence time window and the temporal response of the cold-wire. Time-mean axial and radial velocities, axial and radial turbulent intensities, the single-point cross-correlation between axial and radial velocity fluctuations (~axial Reynolds shear stress), and single-point cross-correlations between axial velocity and temperature fluctuations (~axial turbulent heat flux) and radial velocity and temperature fluctuations (~radial turbulent heat flux) were measured. Results are reported for Reynolds numbers at channel inlet of 22,800, 31,500, and 46,400 at annulus inner wall heat fluxes of 0, 9000 and 16,000 W m^{-2}. The measured radial turbulent heat flux distribution is compared with that calculated from an approximate form of the thermal energy balance equation in which the measured mean velocity and temperature values are used. Also reported is the radial distribution of turbulent Prandtl number estimated from the measurements.

1. Introduction

Turbulent flow and heat transfer in concentric annular channels have been studied extensively because of its many applications in engineering equipment. A distinctive feature of the flow is the radial asymmetry of the velocity field – the smaller the radius ratio, r_i/r_o, the more asymmetric the flow. It is also known that when the inner wall of the channel is heated and the outer wall is not, the asymmetry in the velocity field is enhanced relative to the isothermal condition.

Experiments have been performed by a number of investigators. Heikal et al. [1] measured the velocity field and wall heat transfer rate in flow of air. Kuzay and Scott [2] measured the wall heat transfer rate and mean temperature distribution in air flow. In an earlier effort in our laboratory, Velidandla et al. [3], the velocity field in a vertical annular channel whose inner wall only was heated was measured by a two-component laser Doppler velocimeter (LDV). The ellipsoidal LDV measuring volume (m.v.) had dimensions of 100 μm diameter and 1 mm spanwise length. The coincidence time window was in the 500 μs – 1 ms range. Later, we proposed velocity and temperature wall laws for such a channel [4].

There have been several studies regarding the influence of the LDV m.v. size and coincidence time window on fluid velocity field measurement – for example, [5–7]. Although no significant influence of these parameters was found on the measured mean velocity and turbulence intensities, the axial Reynolds shear stress was significantly affected. The smallest m.v. size yielded the best Reynolds shear stress measurement. A coincidence time window of the order of the fluid transit time through the m.v. was found to be optimal.

Measurement of the turbulent heat flux in the fluid has proved to be difficult. No prior measurement of this quantity in annular channel flow could be found by us.

* Corresponding author. Tel.: +1-480-965-1482; fax: +1-480-963-1384.

E-mail address: roy@asu.edu (R.P. Roy).

0017-9310/01/$ - see front matter
PII: S0017-9310(00)00150-2

Nomenclature

C_P	specific heat of the fluid at constant pressure
D_h	channel hydraulic diameter, $2(r_o - r_i)$
g	acceleration due to gravity
Gr, Gr_q	Grashof numbers, $\beta g(\overline{T}_{wi} - \overline{T}_b)D_h^3/v^2$, $\beta g D_h^4 q''_w/\lambda v^2$
k	turbulent kinetic energy per unit mass of fluid
P	mean pressure
Pr	molecular Prandtl number
Pr_t	turbulent Prandtl number
q''_w	wall heat flux
r	radial coordinate
R^*	dimensionless radius, $(r - r_i)/r_o - r_i)$
R_m	radial location of maximum mean axial velocity
R_0	radial location of zero axial turbulent shear stress
Re	Reynolds number, $\overline{U}_b D_h/v$, based on fluid properties at $\overline{T}_{in}$
$\overline{T}$, $\overline{T}_b$	time-mean liquid temperature, time-mean liquid bulk temperature
t, t'	temperature fluctuation, temperature fluctuation intensity
$\overline{U}$, $\overline{V}$	time-mean axial velocity, time-mean radial velocity
u, v, w	axial, radial, azimuthal velocity fluctuation
u', v'	axial, radial turbulent intensity
U_τ	friction velocity, $(\tau_w/\rho)^{1/2}$
$\overline{U}_b$	bulk axial velocity at channel inlet
U^+	time-mean axial velocity in wall coordinate
$\overline{uv}$	single-point cross-correlation between axial and radial velocity fluctuations, = axial Reynolds shear stress divided by ρ
$\overline{ut}$	single-point cross-correlation between axial velocity and temperature fluctuations, = axial turbulent heat flux divided by ρC_P
$\overline{vt}$	single-point cross-correlation between radial velocity and temperature fluctuations, = radial turbulent heat flux divided by ρC_P
y	coordinate normal to the wall
y^+	non-dimensional wall normal coordinate, yU_τ/v
z	axial coordinate

Greek symbols

β	volumetric coefficient of thermal expansion for fluid, $-(1/\rho)(\partial\rho/\partial T)_P$
ϵ	dissipation rate of k per unit mass of fluid
$\hat{\theta}$	uncertainty (percent)
κ	von Karman constant in velocity wall law
κ_H	constant in temperature wall law
λ	thermal conductivity of fluid
v	kinematic viscosity of fluid
ρ	density of fluid
τ_{wi}, τ_{wo}	axial shear stress at inner wall, outer wall
ϕ	azimuthal coordinate

Subscripts

0	reference state; also, zero axial shear stress location
i, o	annular channel inner wall, outer wall
in	channel inlet

In pipes, Hochreiter and Sesonske [8] used constant temperature and constant current anemometry to measure turbulent heat flux in flow of mercury, while Hishida and Nagano [9] employed constant temperature anemometry and cold-wire in air flow. LDV and cold-wire were used by Polyakov and Shindin [10] in flow of air through a heated pipe, Thole and Bogard [11] in air flow over a heated plate, Wardana et al. [12] in air flow through a rectangular channel, and Heist and Castro [13] in stably stratified boundary layer in a wind tunnel. The important issues in turbulent heat flux measurement have been identified to be: spatial resolution of the velocity and temperature sensors, temporal resolution of the sensors, and the separation distance between them relative to the length scales in the flow.

In this study, experiments were conducted in upflow of liquid Refrigerant-113 (R-113) through a vertical concentric annular channel whose inner wall only was heated. Measurements were made at three Reynolds numbers, and at isothermal condition and two uniform wall heat fluxes. Significant improvement was achieved in the axial Reynolds shear stress measurement compared to our earlier effort [3]. The turbulent heat flux measurements are new.

2. The experiments

Fig. 1 shows, schematically, the *measurement section* of the 3.66 m long annular channel. The inner tube of the channel is of 304 stainless steel (i.d. = 14.60 mm, o.d. = 15.78 mm). The outer tube of the 0.521 m long measurement section is made of optical quality quartz (i.d. = 38.02 mm, o.d. = 42.02 mm). The *measurement plane (m.p.)* was located 0.424 m ($\approx$ 19 hydraulic diameters) downstream of the measurement section entrance, this entrance in turn being 1.56 m downstream of the beginning of the 2.75 m heated length. The inner

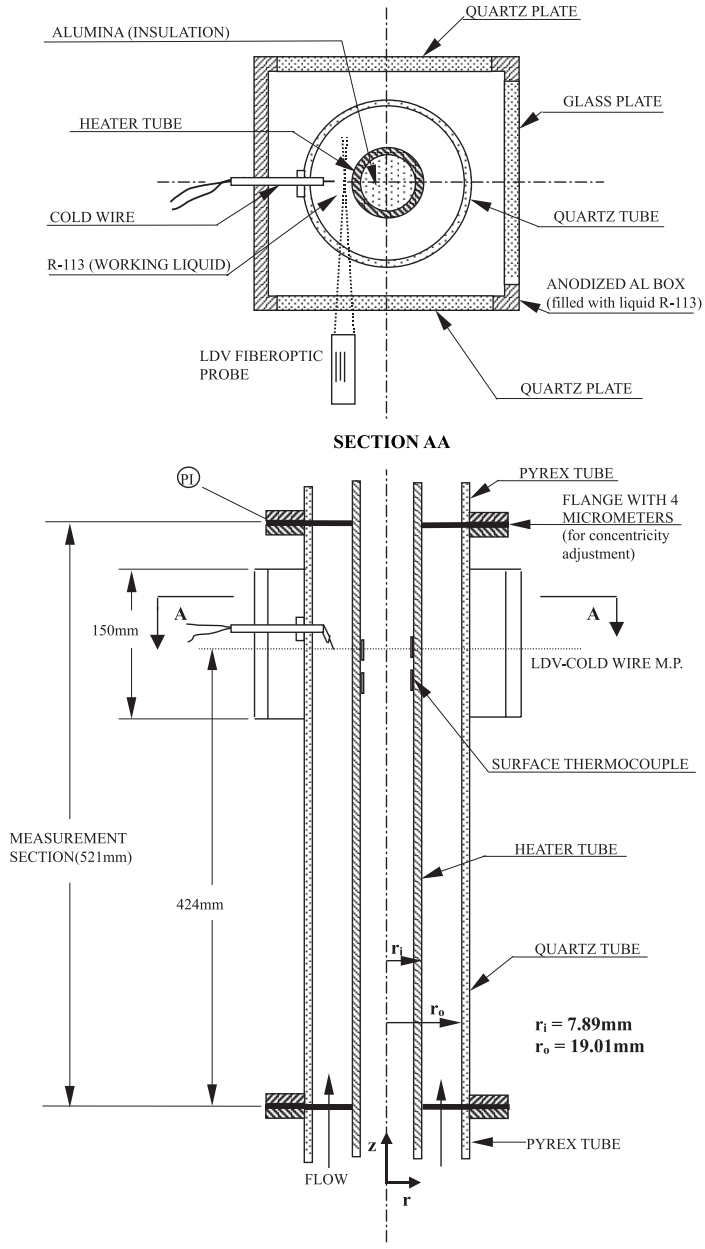

Fig. 1. The measurement section.

stainless tube can be heated over the latter length by direct current. A 0.91 m unheated section is provided upstream of the heated length. Additional information about the annular channel and the experimental rig can be found in [3].

An anodized aluminum box with flat front and back quartz windows and a glass side window served as a jacket around a 15 cm length of measurement section (Fig. 1). The box was filled with liquid R-113 to alleviate laser beam refraction at the outer wall of the quartz tube.

The volumetric flow rate of liquid R-113 through the channel was measured by a turbine flow meter (EG&G Flow Technology). The liquid temperature at the test section inlet was measured by a copper–constantan thermocouple (Omega). The pressure at the m.p. was measured by a test gauge (Omega, 0–1200 kPa range, 1.4 kPa resolution).

Four copper–constantan surface thermocouples (RdF Corporation) were installed on the inner wall of the heater tube which was then filled with aluminum oxide powder insulation.

The entire test section except for the length encased by the aluminum box was insulated on the outside with 50 mm thick jacketed fiberglass wool.

2.1. The two-component LDV system

The LDV system (TSI) consists of a 100 mW Argon-ion laser with 50 mm beam spacing and a backscatter light detector. A 130 mm focal length transmitting lens was used for the measurements reported here. This focal length is considerably shorter than the 261 mm length used for the measurements reported in [3]. The current m.v. dimensions are calculated to be 55 μm diameter and 290 μm spanwise length, Fig. 2. Hollow glass spheres 8–12 μm in diameter were used to seed the flow.[1]

A brief discussion of the LDV beam refraction, the beam tracing algorithm required, and the beam steering module which was employed to place the m.v. at desired locations in the annulus is provided in [3].

The coincidence mode was used for the velocity measurements. The coincidence time window is a critical parameter especially for Reynolds shear stress measurement [7]. The general rule is that the time window should be about the same as or slightly larger than the transit time of a seed particle through the LDV m.v. and smaller (by up to an order of magnitude) than the difference between the arrival times of consecutive seed particles at the m.v. For the measurements reported here, the coincidence time window was in the 100–200 μs range.

Data density, defined as the product (data validation rate) × (Taylor time microscale), is an important parameter when considering the presence of statistical bias in the velocity data [14]. In the experiments reported here, the data density was between 2 and 6 – i.e., from intermediate to high. Thus, bias should not be a significant problem.

2.2. The cold-wire

A 3.8 μm diameter tungsten cold-wire was used to measure the liquid temperature field, Fig. 2. While the total wire length was 0.9 mm, only the 0.3 mm bare center segment was the active (temperature-sensing) length, the two side segments (each 0.3 mm long) having been coated with a 5 μm thick copper layer. The cold-wire was operated by a Temperature Module (TSI 1040) which feeds a constant current to the wire from a regulated supply. The amplifier in the module is referenced to ground and operates in a feedback mode to permit zero and gain setting. The output from the module was further amplified by a Pacific Instruments amplifier–filter unit prior to data acquisition.

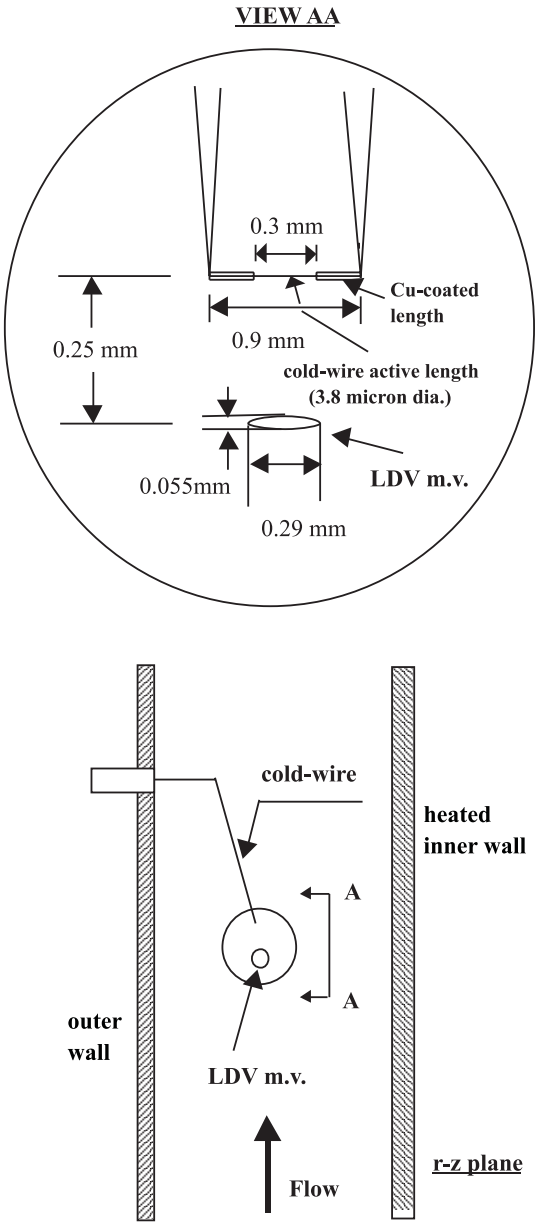

Fig. 2. Positioning of the LDV m.v. with respect to the cold-wire.

The temporal response of the cold-wire in a particular fluid flow depends upon the thermal inertia of the wire, heat conduction from its ends to the relatively massive support prongs, and transport properties of the fluid. Wroblewski and Eibeck [15] suggested an analyt-

[1] Seed particles such as of nylon tended to soften in the heated liquid and then adhere to the cold-wire.

ical method to compensate for the first two effects. Adopting a similar approach, we used an active phase-lead circuit for thermal inertia compensation and a constant gain for the end conduction. The time constant of the compensated cold-wire was measured in situ at the velocities of our interest and found to be 0.30 ± 0.02 ms.

2.3. Simultaneous measurement of local velocity and temperature

Several issues needed to be considered during this measurement. One is the juxtaposition of the LDV m.v. and the active length of the cold-wire. They must be sufficiently close to provide the correct cross-correlation between velocity and temperature fluctuations but, at the same time, not interfere with each other. Referring to Fig. 2, if the LDV m.v. is placed too close to the cold-wire, the latter will be felt by the m.v. as an obstruction to the flow and at least the mean axial velocity will be rendered lower. A lesser problem (in the sense that this occurs at even smaller separation distance) is the heat-up of the cold-wire by the laser beams. In our case, an axial separation distance of 0.25 mm (≈15–30 wall units depending upon the flow rate) was found to be a good choice. An additional consideration for low-velocity flows such as ours is the time delay incurred by the fluid in travelling from the LDV m.v. location to the cold-wire location (200–500 μs for the present experiments). To account for this, a delay circuit was used to introduce the appropriate time delay in the temperature time series data. The DATALINK multi-channel interface (TSI) and a 16-bit data acquisition board were then used to acquire the velocity–temperature data simultaneously. The velocity/temperature sampling points were 36,000 at each measured location. The data rate ranged from about 400 Hz in the region close to the wall to about 800 Hz in the core of the channel.

3. Results and discussion

Selected results from eight experiments are presented. These experiments were conducted at test section inlet temperature of 42.7°C, three different flow rates, and inner wall heat fluxes of zero and two non-zero values. Table 1 contains the experimental conditions and associated uncertainties. In this table and the remainder of the paper, the term "mean" of a quantity implies its "time-mean".

The data are presented in dimensional form because some effects which may be quantitatively small can be identified unambiguously in this form – for example, effects due to modest changes in Reynolds number. Also, when turbulent stresses are non-dimensionalized by the square of the friction velocity, it is difficult to surmise whether their measured values are correct.

Table 1
Conditions for the eight experiments and associated measurement uncertainties

Parameter	Experiment								Uncertainty[a]
	1	2	3	4	5	6	7	8	
Fluid mass velocity (kg/m^2s)	568	568	568	784	784	784	1156	1156	±4
$\overline{U}_{b,in}$ (m/s)/Re_{in}	0.374/22,800	0.374/22,800	0.374/22,800	0.516/31,500	0.516/31,500	0.516/31,500	0.760/46,400	0.760/46,400	±0.003/± 200
R-113 pressure at m.p. (kPa)	269	269	269	269	269	269	269	269	±1
Mean liquid temperature at test section inlet (°C)	42.7	42.7	42.7	42.7	42.7	42.7	42.7	42.7	±0.1
Inner wall heat flux (W/m^2)	0	9000	16,000	0	9000	16,000	0	16,000	±100 (for the non-zero heat fluxes)
Pr at m.p.	7.25	7.15	7.07	7.25	7.18	7.12	7.25	7.16	–
$Gr_{m.p.} \times 10^{-7}$	–	2.21	4.31	–	1.59	2.97	–	2.05	–
$Gr_{q,m.p.} \times 10^{-9}$	–	3.66	6.75	–	3.62	6.60	–	6.47	–
$(Gr/Re^2)_{m.p.}$	–	0.041	0.078	–	0.016	0.029	–	0.009	–
$(Gr_q/PrRe^4)_{m.p.} \times 10^{10}$	–	17.46	30.6	–	4.84	8.51	–	1.81	–

[a] The uncertainty estimate is for 95 % confidence.

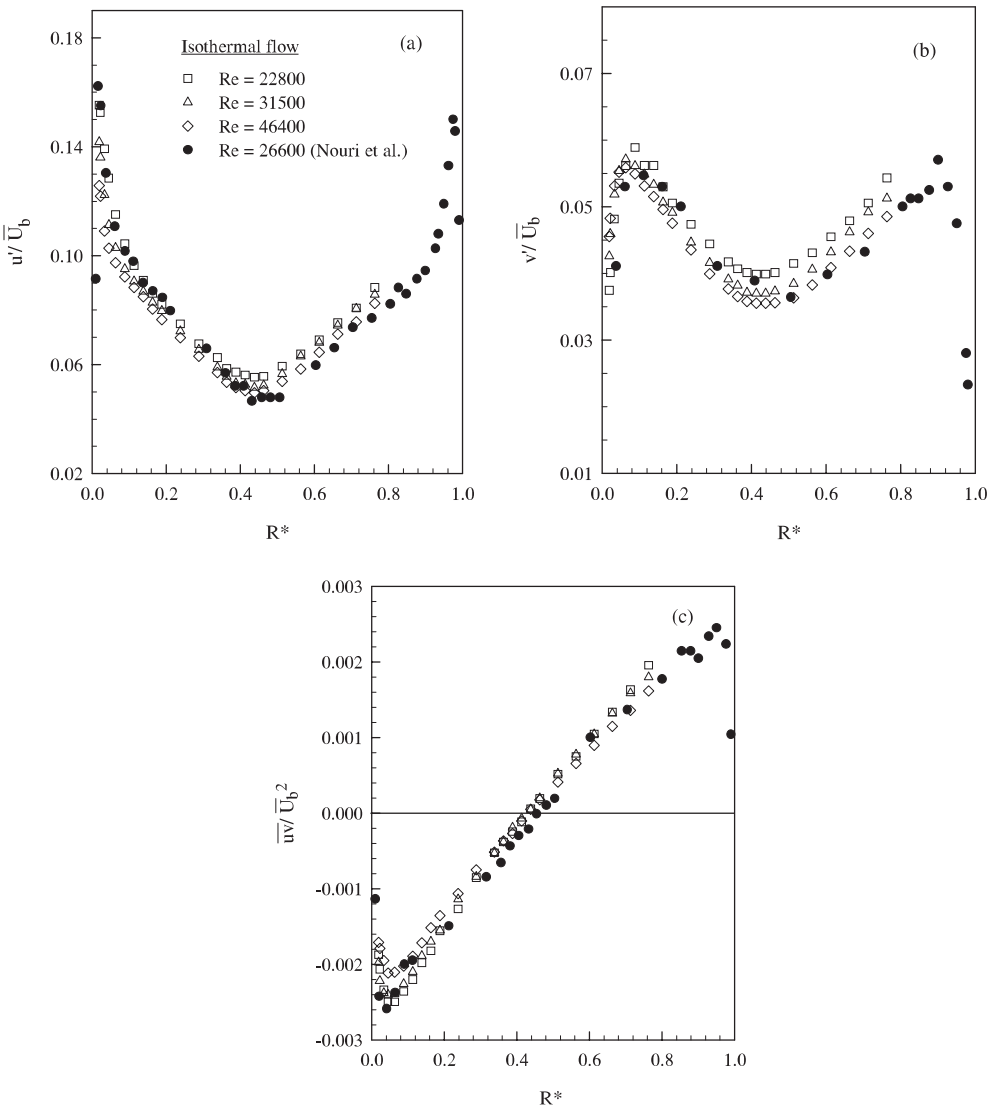

Fig. 3. Comparison with the measurement of Nouri et al. [16], (a) axial turbulent intensity, (b) radial turbulent intensity, (c) axial Reynolds shear stress (divided by ρ).

The data for $\overline{V}$ are not shown since the values were always very small compared to the $\overline{U}$ values ($\lesssim 1\%$). This feature is consistent with the hydrodynamically fully developed condition (for the isothermal experiments) and close to fully developed condition (for the heated experiments) at the measurement plane.

3.1. Velocity field

Nouri et al. [16] reported, among other measurements, LDV measurement of the velocity field in isothermal turbulent flow of a Newtonian fluid in a concentric annular channel of radius ratio 0.500. Since this radius ratio is slightly larger than ours, the velocity field will be slightly less asymmetric than in our isothermal flows. Figs. 3(a)–(c) compare the radial distributions of axial turbulent intensity, radial turbulent intensity, and axial Reynolds shear stress, respectively.[2] The intensities are non-dimensionalized by the bulk axial velocity and the shear stress by the square of this velocity. Keeping in mind the expected difference in asymmetry, the agreement is satisfactory.

[2] The Nouri et al. data were read off the journal figures. As such, some inaccuracy in our plots of the data should be expected.

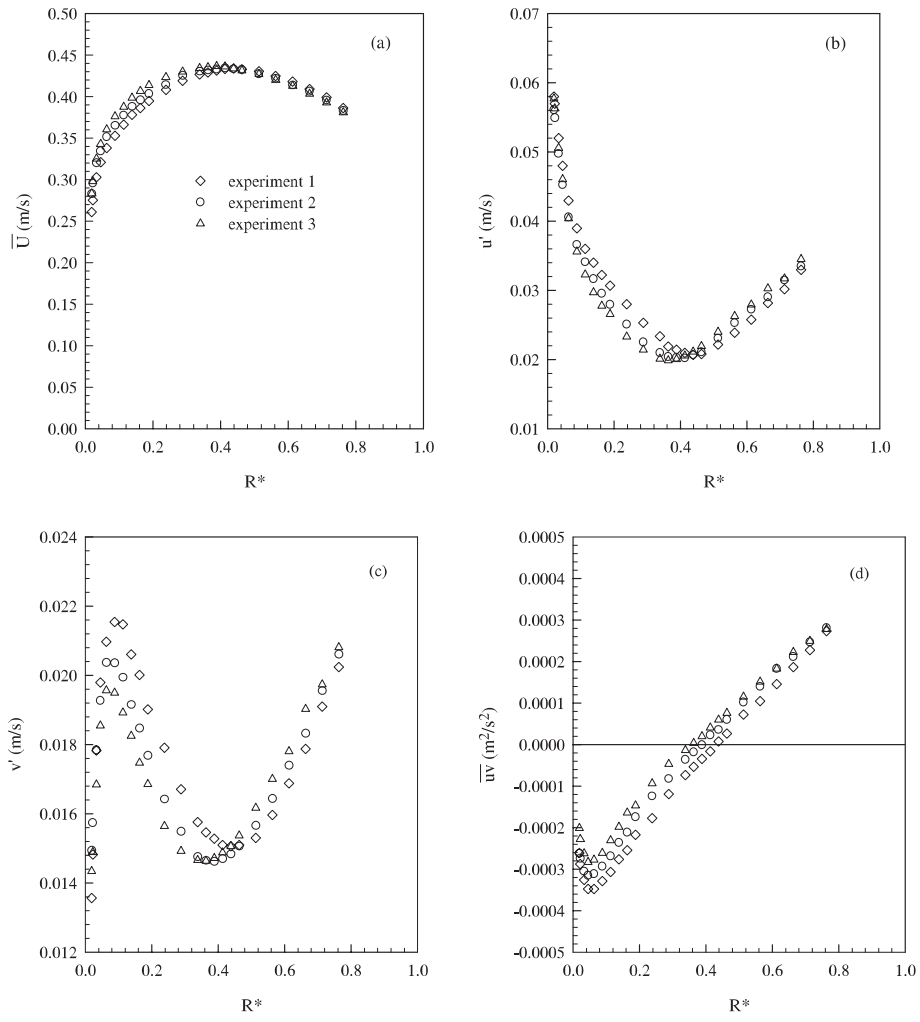

Fig. 4. Velocity field at Reynolds number of 22,800, (a) mean axial velocity, (b) axial turbulent intensity, (c) radial turbulent intensity, (d) axial Reynolds shear stress (divided by ρ).

Figs. 4(a)–(d) show the radial profiles of, respectively, $\overline{U}$, u', v', and $\overline{uv}$ at the m.p. for experiments 1, 2, and 3. Close to the heated wall ($R^* < 0.03$), the profiles tend to merge. However, slightly further from the wall $\overline{U}$ becomes higher as the wall heat flux increases, this trend continuing to $R^* \approx 0.4$. Beyond $R^* \approx 0.5$, $\overline{U}$ decreases slightly as the wall heat flux increases. This, of course, is required for mass conservation. Both u' and v' tend to merge near the heated wall, but slightly farther away they decrease as the wall heat flux increases, this continuing to $R^* \approx 0.42$. Beyond $R^* \approx 0.45$, the intensities increase by a small amount with wall heat flux. The location of maximum $\overline{U}$ as well as the locations of minimum u' and v' shift toward the heated wall as the wall heat flux increases. These trends are similar to those reported in [3]. The one difference is that the v' magnitudes are slightly higher in the present measurements. This is expected since the LDV m.v. is smaller and thus able to capture the smaller scale fluctuations normal to the wall better.

The significant shift of the zero axial Reynolds shear stress location toward the inner wall as the wall heat flux increases is also similar to our observation in [3]. However, in the present measurement the magnitude of $\overline{uv}$ is markedly larger near the inner wall compared to [3]. This is also an improvement brought about by the smaller LDV m.v. and the narrower (and more appropriate) coincidence time window.

Figs. 5(a)–(d) show the radial profiles of the same four quantities, viz., $\overline{U}$, u', v', and $\overline{uv}$, for experiments 4, 5, and 6. The trends remain the same but the changes in the velocity field due to imposition of wall heat flux are smaller at this higher flow rate. Figs. 6(a)–(d) show the radial profiles of $\overline{U}$, u', v', and $\overline{uv}$ for experiments 7 and 8.

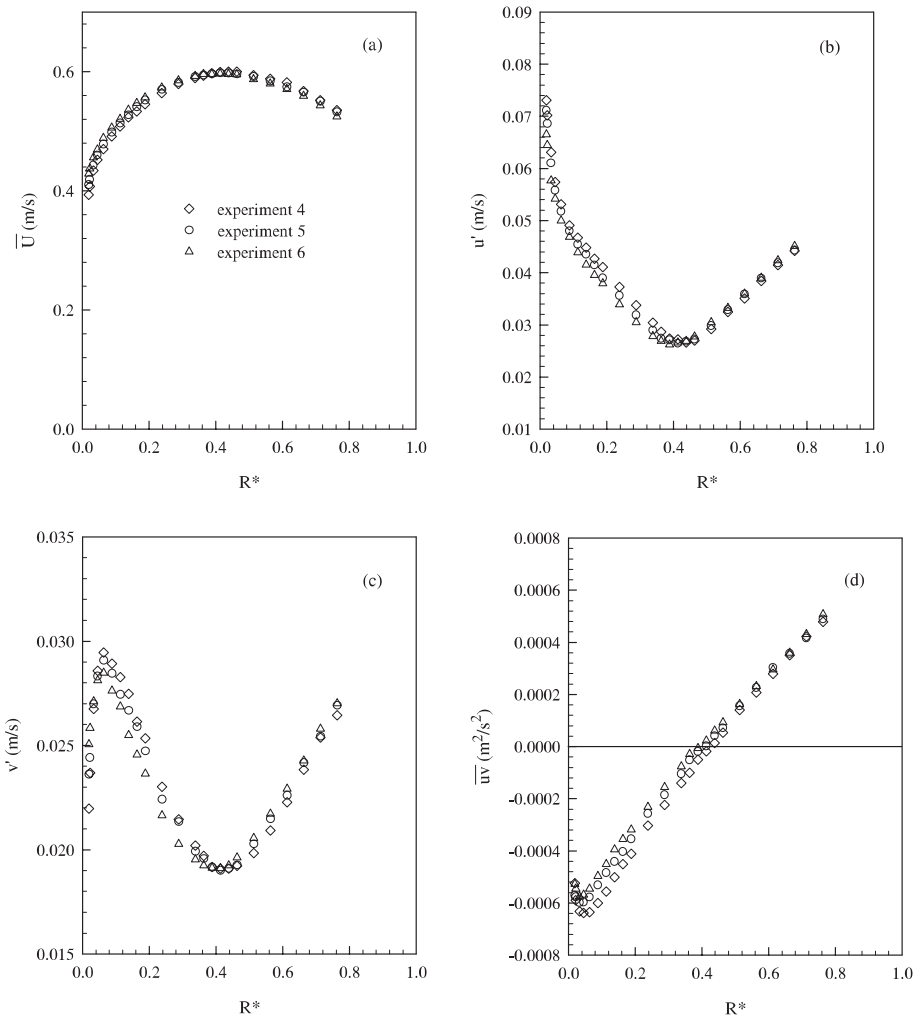

Fig. 5. Velocity field at Reynolds number of 31,500, (a) mean axial velocity, (b) axial turbulent intensity, (c) radial turbulent intensity, (d) axial Reynolds shear stress (divided by ρ).

Again, the trends are the same but the changes caused by wall heat flux are even smaller at this high flow rate.

Our mean axial velocity data for $y^+ \gtrsim 30$ agree well with the wall law proposed in [4].

3.2. Thermal field

Figs. 7(a)–(d) show the radial profiles of, respectively, $\overline{T}$, t', $\overline{ut}$, and $\overline{vt}$ at the m.p. for experiments 2 and 3. In Fig. 7(a), the mean inner wall temperature is also shown. Both the mean liquid temperature and temperature fluctuation intensity increase sharply near the heated wall. A notable feature of the mean temperature profiles is their approximately linear variation in the region $0.15 \lesssim R^* \lesssim 0.4$. The temperature fluctuation intensity profiles exhibit a plateau in the same region, except at low Reynolds numbers in conjunction with a high wall heat flux – for example, experiment 3. If the magnitude of temperature fluctuation at any location in the flow is considered to be proportional to the radial gradient of the mean temperature there, then the observed features are consistent.

Two characteristics should be noted in Fig. 7(c): (i) the magnitude of $\overline{ut}$ increases with the wall heat flux in all regions except far from the heated inner wall ($R^* \gtrsim 0.8$) where it tends to not change markedly, and (ii) the zero crossing location of $\overline{ut}$ coincides approximately with the location of the maximum in the mean axial velocity profile. The first feature may be explained as being due to the increase in temperature fluctuation intensity at higher wall heat flux (assuming that the correlation coefficient between u and t remains the same). The second feature is explainable by considering the radial transport of fluid 'particles' carrying the local

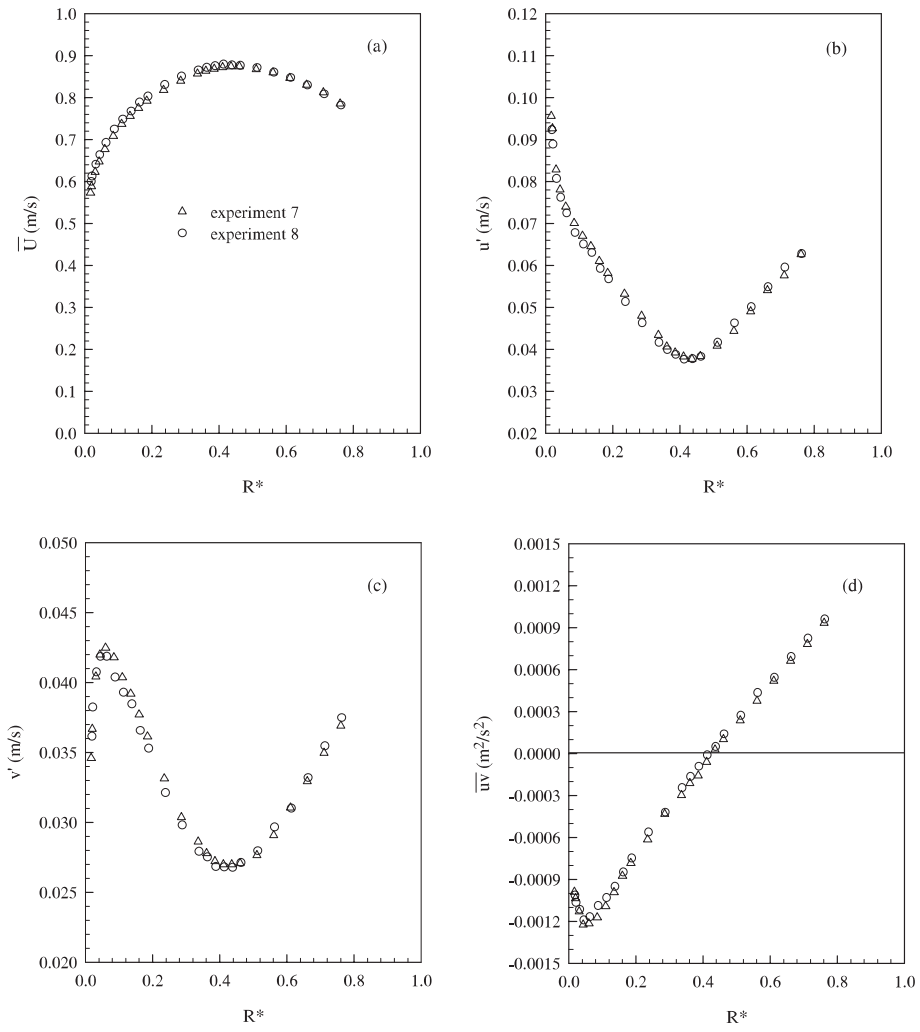

Fig. 6. Velocity field at Reynolds number of 46,400, (a) mean axial velocity, (b) axial turbulent intensity, (c) radial turbulent intensity, (d) axial Reynolds shear stress (divided by ρ).

instantaneous axial velocity and temperature from various radial locations to any particular location, and the resulting sign of $\overline{ut}$ at the latter location.

In Fig. 7(d), plotted along with the measured $\overline{vt}$ is the radial profile of the same quantity calculated from thermal energy balance at the axial plane in the channel:

$$\frac{[\overline{vt}]_r}{q''_w/(\rho C_P)} = \frac{r_i \int_r^{r_o} \overline{U}(r) r\,dr}{r \int_{r_i}^{r_o} \overline{U}(r) r\,dr} + \frac{\lambda}{q''_w}\left[\frac{\partial \overline{T}}{\partial r}\right]_r + \frac{\rho C_P}{r q''_w}\left[\int_r^{r_o} \overline{V}\frac{\partial \overline{T}}{\partial r} r\,dr + \int_r^{r_o} \frac{\partial(\overline{wt})}{\partial \phi}\,dr + \int_r^{r_o} \frac{\partial(\overline{ut})}{\partial z} r\,dr\right]. \quad (1)$$

The terms on the right-hand side of this equation are arranged in descending order of magnitude. Neglecting the three terms given in the underbrace as small, $\overline{vt}$ is calculated using the measured local values of $\overline{U}$ and $\overline{T}$.

The difficulty encountered in measuring $\overline{vt}$ close to the inner wall is evident from Fig. 7(d). The measured value peaks at $R^* \approx 0.07$–0.08 and then drops off sharply closer to the wall. The energy balance equation, on the other hand, predicts the peak to be at $R^* \approx 0.02$–0.03 which is more realistic. The undermeasurement of $\overline{vt}$ close to the wall is quite possibly due to: (i) the spatial averaging of the small-scale velocity and temperature fluctuations over the spanwise lengths of, respectively, the LDV m.v. and the cold-wire active length, and (ii) the loss of cross-correlation caused by the separation distance between the LDV m.v. and the cold-wire. It should be noted that when the fluid Prandtl number is greater than 1 (see Table 1), the smallest temperature

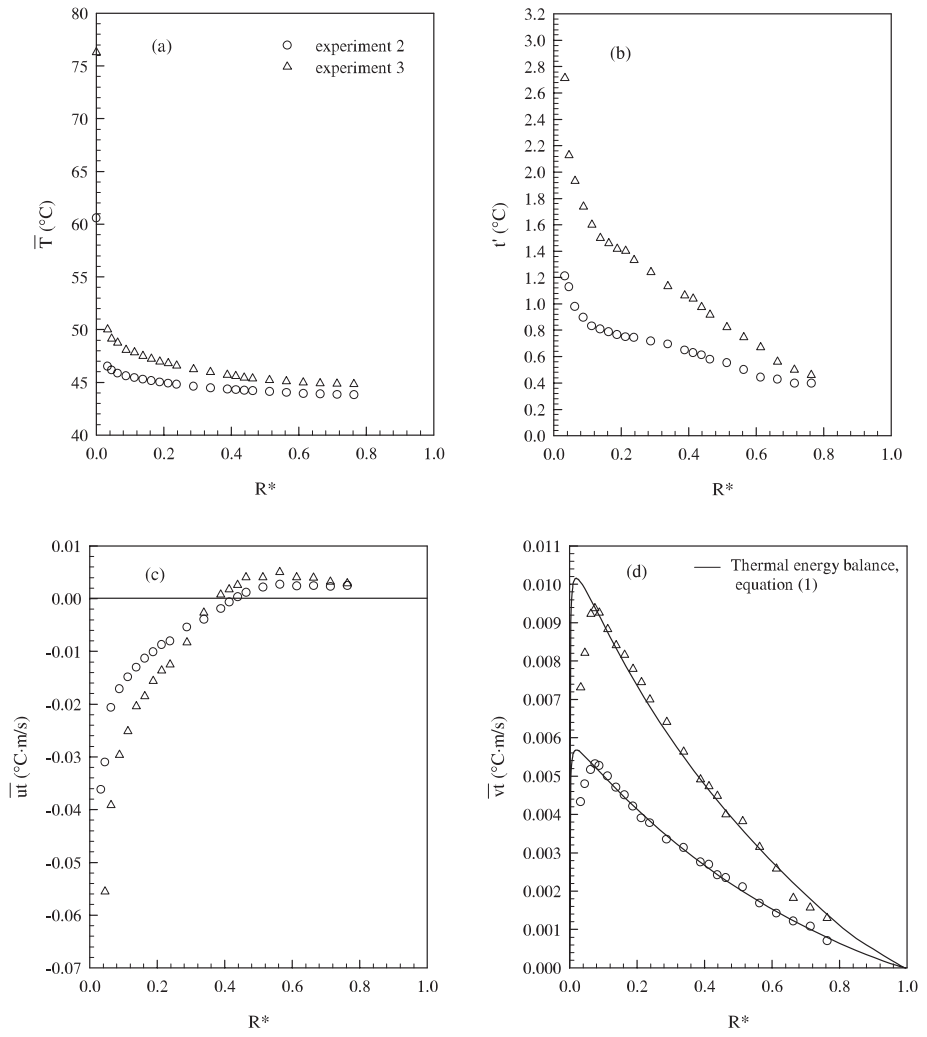

Fig. 7. Temperature field at Reynolds number of 22,800, (a) mean temperature, (b) temperature fluctuation intensity, (c) axial turbulent heat flux (divided by ρC_P), (d) radial turbulent heat flux (divided by ρC_P).

length scales are smaller than the smallest velocity scales [17]. An additional cause for the undermeasurement of $\overline{vt}$ may be the time constant of the cold-wire (a smaller time constant would be preferable), although this probably is not as much of a problem as the spatial scales and probe dimensions.

Figs. 8(a)–(d) contain the radial profiles of, respectively, $\overline{T}$, t', $\overline{ut}$, and $\overline{vt}$ for experiments 5 and 6. The same trends as in Fig. 7 are displayed by the data. Figs. 9(a)–(d) show the radial profiles of the same four quantities for experiment 8. Again, the trends are similar.

In [4], we reported a logarithmic wall law for the mean fluid temperature at conditions where $(Gr_q/PrRe^4)_{m.p.}$ has modest values (typically less than 10^{-9}), i.e., the buoyancy effect is not particularly strong. Of the five heated experiments reported in the present paper, only three satisfy this criterion. Their data fall within the uncertainty range of the law proposed in [4] albeit on the low side.

We now calculate the turbulent Prandtl number, Pr_t, from our measurements by two different methods. First, it is equated to the ratio κ/κ_H yielding the value 0.91 ± 0.04. This is shown in Fig. 10. Second, we use the relation

$$Pr_t = \frac{\overline{uv}}{\overline{vt}} \cdot \frac{\partial \overline{T}/\partial r}{\partial \overline{U}/\partial r}. \tag{2}$$

Best-fit expressions of the measured data are used for $\overline{T}$, $\overline{U}$, $\overline{uv}$, and $\overline{vt}$. Since the calculated gradients of $\overline{T}$ and $\overline{U}$ are very sensitive to the respective expressions, considerable care is needed in obtaining these. In contrast to the first method, local values of Pr_t are obtained. The

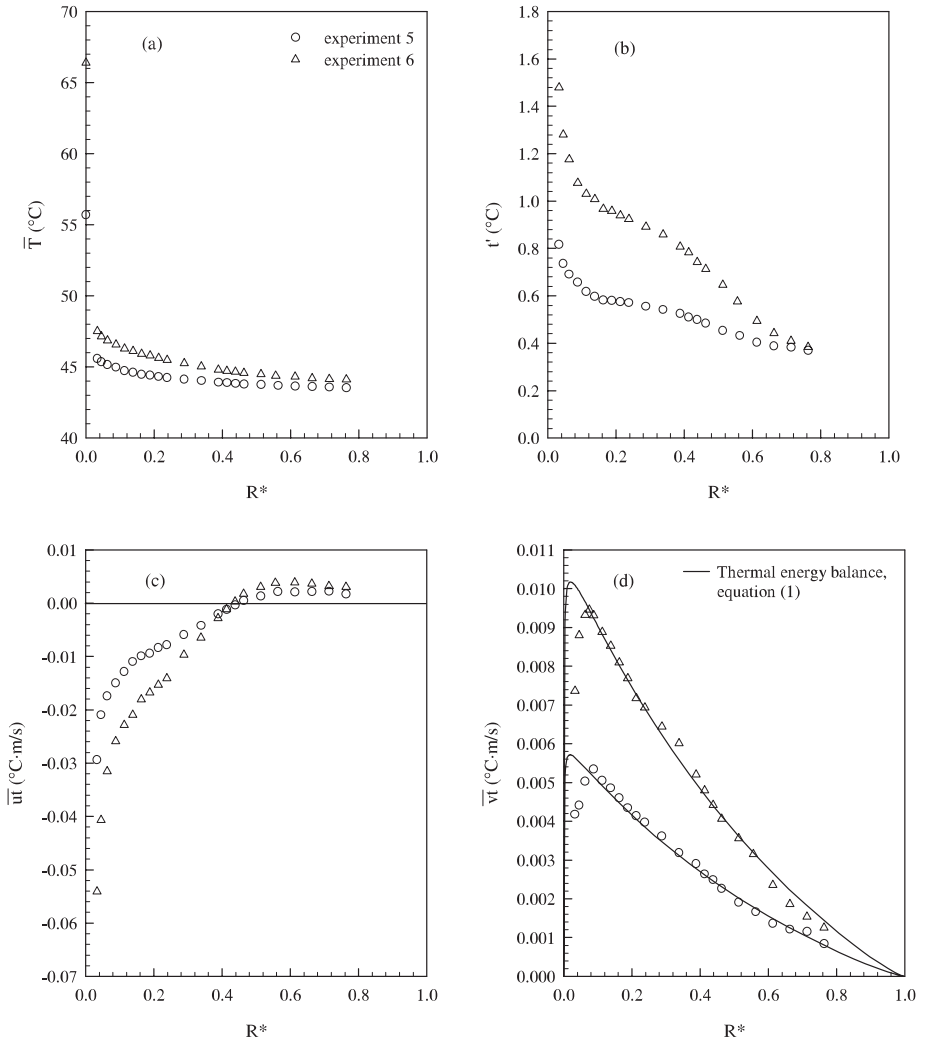

Fig. 8. Temperature field at Reynolds number of 31,500, (a) mean temperature, (b) temperature fluctuation intensity, (c) axial turbulent heat flux (divided by ρC_P), (d) radial turbulent heat flux (divided by ρC_P).

results are shown in Fig. 10. Pr_t obtained by this procedure is indeterminate in a narrow radial zone for each experiment. This zone is delimited by the $\overline{uv} = 0$ and $\partial\overline{U}/\partial r = 0$ locations and the Pr_t values shown here are to be disregarded. The greater than unity values of Pr_t near the inner wall are meaningful. This is a result of the near-wall behavior of the four quantities which define Pr_t, Eq. (2), as suggested by Slanciuskas and Pedisius [18].

The uncertainties in the measured turbulent quantities and the turbulent Prandtl number were estimated following Benedict and Gould [19]. The estimated uncertainty values (percent) at a 95% confidence level are:

$\hat{\theta}_{u'}$	$\hat{\theta}_{v'}$	$\hat{\theta}_{\overline{uv}}$	$\hat{\theta}_{t'}$	$\hat{\theta}_{\overline{ut}}$	$\hat{\theta}_{\overline{vt}}$	$\hat{\theta}_{Pr_t}$
<1.0	<1.0	<3.5	<1.0	<2.5	<5.0	<6.0

At this juncture, a discussion of the velocity and thermal fields is in order. In [3], we had discussed the effect of buoyancy on the velocity field on the basis of two mechanisms suggested by Petukhov and Polyakov [20] – the *external effect* and the *structural effect*. The first effect is due to the buoyancy force acting on the entire flow and is represented by $(\rho - \rho_0)g_i$ in the i-momentum equation.[3] The second effect arises from the turbulent density fluctuations in the gravitational field and is represented by the production term $(-g_i\beta\overline{u_i t})$ in the turbulent kinetic energy equation. According to Petukhov and Polyakov, the two mechanisms appear

[3] This equation is given in Part II of this two-part paper.

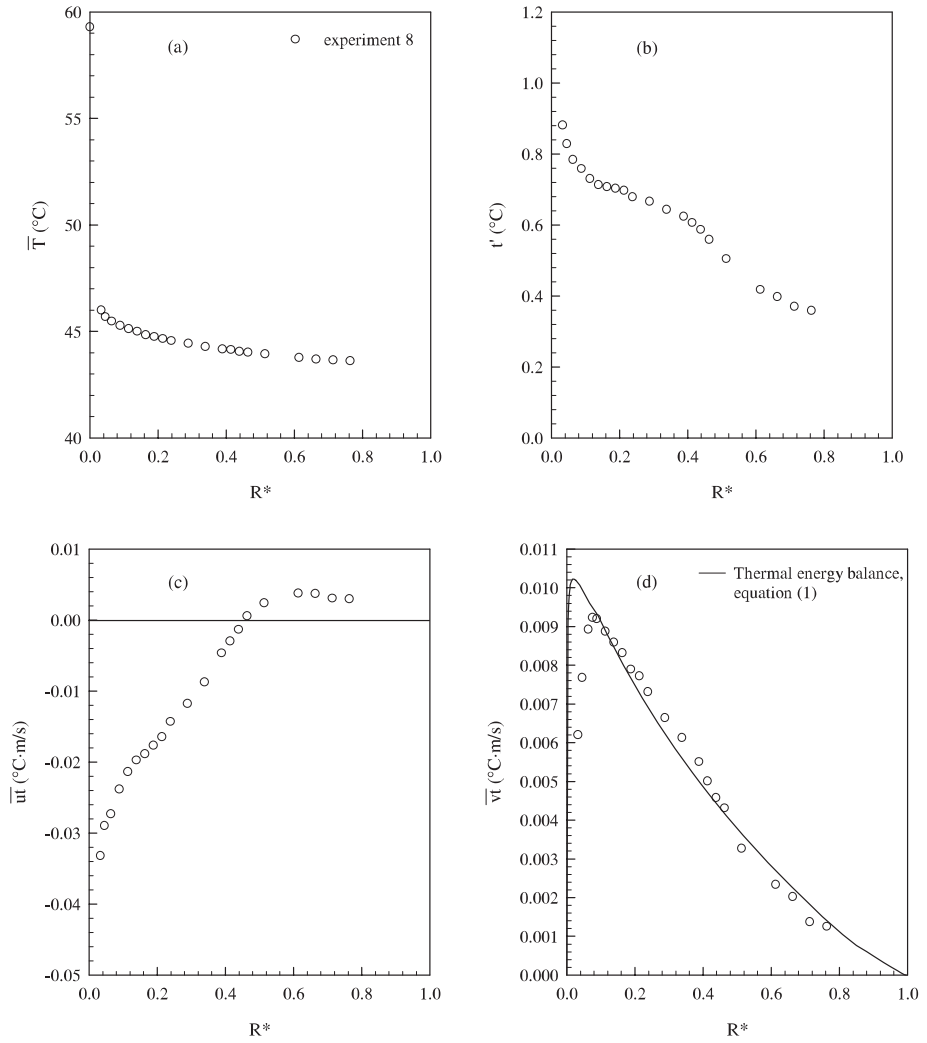

Fig. 9. Temperature field at Reynolds number of 46,400, (a) mean temperature, (b) temperature fluctuation intensity, (c) axial turbulent heat flux (divided by ρC_P), (d) radial turbulent heat flux (divided by ρC_P).

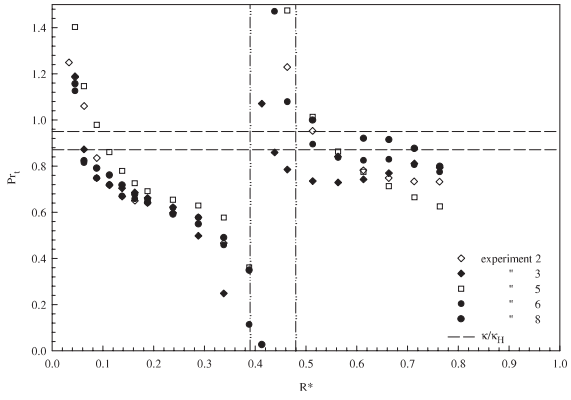

Fig. 10. Turbulent Prandtl number.

simultaneously in the flow and their effects can be similar or dissimilar.

In the heated experiments, the turbulent kinetic energy production due to mean shear, $-\overline{uv}(\partial\overline{U}/\partial r)$, is estimated to be an order of magnitude larger than the production due to buoyancy. From this consideration, the external effect was more important.

If we integrate the axial momentum equation from the inner wall to any radial position in the annulus, the following equation is obtained:

$$\left(\mu\frac{\partial\overline{U}}{\partial r}-\rho\overline{uv}\right)-\frac{1}{r}\int_{r_i}^{r}\rho_0 g\beta\left(\overline{T}_0-\overline{T}\right)r\,\mathrm{d}r = \frac{r_i}{r}\tau_{w_i}-\left(-\frac{1}{2}\frac{\mathrm{d}P'}{\mathrm{d}z}\right)\frac{r^2-r_i^2}{r}, \tag{3}$$

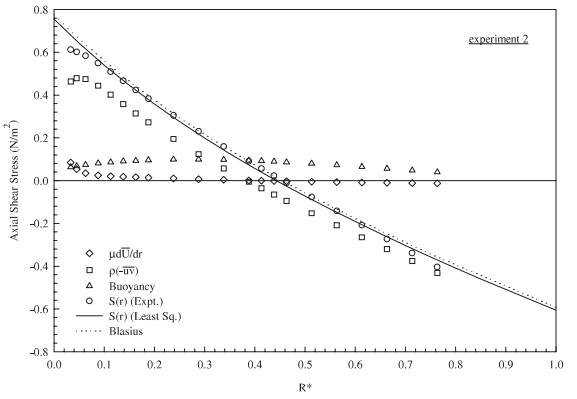

Fig. 11. Axial shear stress balance in the flow at the measurement plane for experiment 2.

where $P' = P + \rho_0 gz$, $\overline{T}_0$ is a reference temperature given by $2/(r_o^2 - r_i^2)\int_{r_i}^{r_o} \overline{T} r\,dr$, and the axial pressure gradient is $dP'/dz = -2(r_i\tau_{wi} + r_o\tau_{wo})/(r_o^2 - r_i^2)$. The right-hand side of Eq. (3) can be expressed as $\tau_{wi}A_1(r) + \tau_{wo}A_2(r)$ where $A_1(r)$ and $A_2(r)$ are known functions of r.

The terms on the left-hand side of Eq. (3) were evaluated using the experimental data. They are plotted in Fig. 11 for experiment 2 as is their sum $S(r)$. A least square fit of the $S(r)$ data (excluding the two points closest to the inner wall) is plotted as well. Also shown in Fig. 11 is the sum of the right-hand side terms of Eq. (3) where τ_{wi} was evaluated using the measured zero $\overline{uv}$ location, R_0, and the pressure gradient was evaluated using the Blasius friction factor formula [4]. The external effect of Petukhov and Polyakov is represented by the buoyancy term in Eq. (3). Fig. 11 indicates that this term contributes significantly to the stress balance in the flow and that it is dominant in the region near R_0. These features were common to all of the heated flows reported here.

It is observed that the effects of buoyancy on the velocity field manifest away from the walls first. The inner and outer boundaries of the affected region move away from the respective walls as the Reynolds number increases. Near the walls, the velocity field does not change significantly due to the substantial viscous forces present.

The thermal field is affected by buoyancy, its influence becoming significant at values of Gr/Re^2 larger than those at which the velocity field begins to be influenced. This is consistent with Polyakov [21].

From the transport equations for the turbulent heat flux components, the following algebraic expressions for $\overline{vt}$ and $\overline{ut}$ can be obtained assuming local equilibrium and employing the thin shear layer approximation [20]:

$$\overline{vt} = -D_1 \frac{k}{\epsilon}\overline{v^2}\frac{\partial \overline{T}}{\partial r}, \tag{4}$$

$$\overline{ut} = D_1 \frac{k}{\epsilon}\left[-\overline{uv}\frac{\partial \overline{T}}{\partial r} - D_2\overline{vt}\frac{\partial \overline{U}}{\partial r} + D_3\beta g\overline{t^2}\right], \tag{5}$$

where D_1, D_2, and D_3 are constants. Only the expression for $\overline{ut}$ contains an explicit buoyancy term. Estimates, using the experimental data, of the three terms on the right-hand side of Eq. (5) indicate that $D_3\beta g\overline{t^2}$ is very small in magnitude compared to the other two terms except in the region between R_0 and R_m where their magnitudes are of the same order.

4. Concluding remarks

We have measured the velocity and thermal fields in isothermal and heated turbulent upflow of liquid Refrigerant-113 through a vertical concentric annular channel. The radial distributions of the mean axial and radial velocities, the corresponding turbulent intensities, and the axial Reynolds shear stress were measured at one axial plane in the channel. In the heated flows, the radial distributions of mean temperature, temperature fluctuation intensity, axial turbulent heat flux, and radial turbulent heat flux were measured at the same axial plane. A two-component LDV system was used for the velocity measurements and a cold-wire for the temperature measurements. Use of an LDV measuring volume smaller than that used in our earlier effort in conjunction with a more appropriate coincidence time window enabled improved measurement of the axial Reynolds shear stress close to the inner wall of the annulus. Accurate measurement of the radial turbulent heat flux near the heated inner wall was hindered by the relatively large spanwise length of the LDV measuring volume and the active length of the cold-wire, as well as by the larger than desirable separation distance between the LDV measuring volume and the cold-wire.

The turbulent Prandtl number in the flow was calculated from the measurements by two methods: (1) using the logarithmic wall laws for mean axial velocity and temperature that the respective data comply with, and (2) using the turbulent diffusivities of momentum and thermal energy obtained from the data. The second method yields local turbulent Prandtl number whereas the first method provides a single value which is then considered to be invariant across the channel gap.

Of the external and structural effects of buoyancy on heated flow suggested by Petukhov and Polyakov, the former effect is estimated to be more important for the experiments reported here.

Acknowledgements

This research was supported by National Science Foundation, Thermal Systems Program, Division of Chemical and Thermal Systems, under grant no.

CTS-9411898. Funding from Electric Power Research Institute and Electricité de France is also gratefully acknowledged. Funding for J.A. Zarate was provided by Consejo Nacional de Ciencia y Tecnologia, Mexico.

References

[1] M.R.F. Heikal, P.J. Walklate, A.P. Hatton, The effect of free stream turbulence level on the flow and heat transfer in the entrance region of an annulus, Int. J. Heat Mass Transfer 20 (1976) 763–771.

[2] T.M. Kuzay, C.J. Scott, Turbulent heat transfer studies in annulus with inner cylinder rotation, ASME J. Heat Transfer 99 (1977) 12–19.

[3] V. Velidandla, S. Putta, R.P. Roy, Turbulent velocity field in isothermal and heated liquid flow through a vertical annular channel, Int. J. Heat Mass Transfer 39 (1996) 3333–3346.

[4] J.A. Zarate, M. Capizzani, R.P. Roy, Velocity and temperature wall laws in a vertical concentric annular channel, Int. J. Heat Mass Transfer 41 (1998) 287–292.

[5] T.S. Luchik, W.G. Tiedermen, Timescale and structure of ejections and bursts in turbulent channel flows, J. Fluid Mech. 174 (1987) 529–552.

[6] J.G. Eriksson, R.I. Karlsson, An investigation of the spatial resolution requirements for two-point correlation measurements using LDV, Exp. Fluids 18 (1995) 393–396.

[7] S. Kang, B.K. Patil, R.P. Roy, Effects of coincidence time window and measuring volume size on LDV measurements of turbulence in a liquid flow, accepted for publication in Exp. Fluids, 2000.

[8] L.E. Hochreiter, A. Sesonske, Turbulence structure of isothermal and non-isothermal liquid metal pipe flow, Int. J. Heat Mass Transfer 17 (1974) 113–123.

[9] M. Hishida, Y. Nagano, Simultaneous measurements of velocity and temperature in non-isothermal flows, ASME J. Heat Transfer 100 (1978) 340–345.

[10] A.F. Polyakov, S.A. Shindin, Development of turbulent heat transfer over the length of vertical tubes in the presence of mixed air convection, Int. J. Heat Mass Transfer 31 (1988) 987–992.

[11] K.A. Thole, D.G. Bogard, Simultaneous temperature and velocity measurements, Measure. Sci. Technol. 5 (1994) 435–439.

[12] I.N.G. Wardana, T. Ueda, M. Mizomoto, Velocity–temperature correlation in strongly heated channel flow, Exp. Fluids 18 (1995) 454–461.

[13] D.K. Heist, I.P. Castro, Combined laser-Doppler and cold-wire anemometry for turbulent heat flux measurement, Exp. Fluids 24 (1998) 375–381.

[14] R.V. Edwards, Report of the special panel on statistical particle bias problems in laser anemometry, ASME J. Fluids Engrg. 109 (1987) 89–93.

[15] D.E. Wroblewski, P.A. Eibeck, A frequency response compensation technique for cold wires and its application to a heat flux probe, Exp. Thermal Fluid Sci. 4 (1991) 452–463.

[16] J.M. Nouri, H. Umur, J.H. Whitelaw, Flow of Newtonian and non-Newtonian fluids in concentric and eccentric annuli, J. Fluid Mech. 253 (1993) 617–641.

[17] H. Tennekes, J.L. Lumley, A First Course in Turbulence, 1st ed., MIT Press, Cambridge MA, 1972.

[18] A.A. Slanciuskas, A.A. Pedisius, Nature of turbulent heat transfer with $Pr > 1$, in: O.G. Martynenko, A.A. Zukauskas (Eds.), Heat Transfer: Soviet Reviews, vol. 1, Hemisphere, New York, 1989, pp. 97–210.

[19] L.H. Benedict, R.D. Gould, Towards better uncertainty estimates for turbulence statistics, Exp. Fluids 22 (1996) 129–136.

[20] B.S. Petukhov, A.F. Polyakov, in: B.E. Launder (Ed.), Heat Transfer in Turbulent Mixed Convection, Hemisphere, New York, 1988.

[21] A.F. Polyakov, Transient effects due to thermogravity in turbulence and heat transfer, Heat Transfer – Sov. Res. 11 (1973) 90–98.